Stem Cell Research & Therapy

RESEARCH Open Access

Adipose-derived stem cells apoptosis rejuvenate radiation-impaired skin in mice via remodeling and rearranging dermal collagens matrix

Yufan Zhu[1], Xu Liu[1], Xihang Chen[1*] and Yunjun Liao[1*]

Abstract

Background Chronic radiation dermatitis (CRD) is a late consequence of radiation with high incidence in patients receiving radiotherapy. Conventional therapies often yield unsatisfactory results. Therefore, this study aimed to explore the therapeutic potential and mechanism of adipose-derived stem cells (ADSCs) for CRD, paving the way for novel regenerative therapies in clinical practice.

Methods Clinical CRD skin biopsies were analyzed to character the pathological changes of CRD skin and guided the animal modeling scheme. Subsequently, an in vivo analysisusing mouse CRD models was conducted to explore their effects of ADSCs on CRD, monitoring therapeutic impact for up to 8 weeks. Transcriptome sequencing and histologic sections analysis were performed to explore the potential therapeutic mechanism of ADSCs. Following observing extensive apoptosis of transplanted ADSCs, the therapeutic effect of ADSCs were compared with those of apoptosis-inhibited ADSCs. Multiphoton imaging and analysis of collagen morphologic features were employed to explain how translated ADSCs promote collagen remodeling at the microscopic level based on the contrast of morphology of collagen fibers.

Results Following injection into CRD-afflicted skin, ADSCs therapy effectively mitigated symptoms of CRD, including acanthosis of the epidermis, fibrosis, and irregular collagen deposition, consistent with the possible therapeutic mechanism suggested by transcriptome sequencing. Notably, in vivo tracking revealed a significant reduction in ADSCs number due to extensive apoptosis. Inhibiting apoptosis in ADSCs partially tempered their therapeutic effects. Mechanically, analysis of collagen morphologic features indicated that translated ADSCs might promote dermal extracellular matrix remodeling through enlarging, lengthening, crimping, and evening collagen, counteracting the atrophy and rupture caused by irradiation.

Conclusions This study demonstrated that ADSCs underwent substantial apoptosis upon local skin transplantation, and paradoxically, this apoptosis is essential for their efficacy in promoting the regeneration of late radiation-impaired

*Correspondence:
Xihang Chen
Xihangchen@hotmail.com
Yunjun Liao
yunjun1000@sina.com

Full list of author information is available at the end of the article

skin. Mechanically, transplanted ADSCs could promote the remodeling and rearrangement of radiation-damaged dermal collagen matrix.

Keywords Adipose-derived stem cells, Apoptosis, Chronic radiation dermatitis, Collagen remodeling, Stem cell therapy

Introduction

Radiotherapy is integral to comprehensive cancer treatment, especially breast cancer, yet its common side effect—skin toxicity—poses significant challenges [1, 2]. Nearly 95% of patients undergoing radiotherapy develop radiation dermatitis, [3, 4] a condition encompassing diverse symptoms and pathological changes beyond mere skin inflammation [5]. Chronic radiation dermatitis (CRD), a late consequence, manifests with acanthosis, dermal atrophy, fibrosis, dyspigmentation, telangiectasias, and injury to skin appendages [6, 7]. Abnormal fibroblast activity and irregular collagen deposition directly contribute to dermal atrophy and fibrosis [8, 9].

CRD is typically graded using the toxicity criteria of the Radiation Therapy Oncology Group and the European Organization for Research and Treatment of Cancer (RTOG–EORTC) [10]. Grades 2 and 3 not only impact breast appearance but also induce itching, pain, and, significantly, reduce skin compliance, posing challenges to delayed or delayed-immediate breast reconstruction [11].

The challenge lies in addressing chronic radiation-induced skin fibrosis effectively, as conventional treatments are often unsatisfactory, with treatments such as bioactive dressings, oxygen therapy, growth factors and surgical reconstruction showing limited efficacy and potential complications [12–14]. Recent researches have highlighted the benefit of autologous fat grafting and other fat-derived products in the treatment of chronic radiation-induced skin fibrosis [15–18]. However, the mechanisms by which fat rejuvenate radiation-impaired skin remains to be elucidated but is thought to be driven by the adipose-derived stem cells (ADSCs), increasingly recognized to exert tissue regenerative effects [19–21].

In the present study, we set out to investigate the effect of ADSCs after transplantation on skin repair and regeneration of CRD and its underlying mechanism, paving the way for novel regenerative therapies in clinical practice.

Materials and methods

Human breast skin tissue harvesting

Breast skin tissue samples were obtained respectively from 3 patients undergoing either a lumpectomy or a mastectomy in the Department of Breast Surgery, and 5 patients diagnosed with chronic radiation dermatitis receiving breast reconstruction in Department of Plastic and Cosmetic Surgery, Nanfang Hospital, Guangzhou, China. These tissue samples were embedded into blocks of paraffin wax and cut into thin sections for histological staining.

Human adipose tissue harvesting

Human adipose tissue samples were harvested as discarded tissue from healthy female patients undergoing liposuction in Department of Plastic and Cosmetic Surgery of Nanfang Hospital.

Animals

Seven-week-old male Balb/C mice were purchased from Casgene Biotech company (Guangzhou, China). The mice were cage-housed under specific-pathogen-free conditions (24 °C, 12 h light/dark cycle, and 50% humidity) with free access to food and water. The animal experiments were conducted according to the protocol approved by the Institutional Animal Care and Use Committee of Nanfang Hospital, Southern Medical University (Guangzhou, China). The work has been reported in line with the ARRIVE guidelines 2.0, with additional supporting documents provided in the supplementary materials. At the end of the experiments, euthanasia was performed using sodium pentobarbital, following the American Veterinary Medical Association Guidelines for the Euthanasia of Animals (2020 Edition).

Isolation, culture, and characterization of ADSCs

The harvested human adipose tissue was excised, finely minced, then digested with equal volume of 0.1% collagenase type I (Solarbio, China) on a shaker at a low setting for 50 min at 37℃ in a 50 cm^3 centrifuge tube. After complete dissociation, the tissue sample was added with an equal volume of Dulbecco's modified Eagle medium and Kaighn's modification of Ham's F12 (DMEM-F12 media, Gibco, USA) with 10% fetal bovine serum (FBS, Gibco, USA) to neutralize the collagenase. The cell suspension was centrifuged at 1200 rpm for 3–5 min. The infranatant and resultant pellet were resuspended and passed through a 100-μm mesh filter (Coring Falcon, USA), after which the filtered cell suspension was centrifuged at 800 rpm for 3min. The supernatant was discarded and the pellet was plated in ADSCs culture medium containing DMEM-F12 supplemented with 10% FBS and 1%penicillin–streptomycin (NCM, China) at a density of 1.0×106 nucleated cells per 100mm^2 dish for culture (37℃, 5% CO^2). The medium was replaced every day for the first 3 days the non-adherent cells were discarded. The cells were then passaged every week at a ratio

of 1:3. Further cell experiments were undertaken with ADSCs in the third to fifth passage.

Characterization of ADSCs was described in previous study [22]. Briefly, ADSCs were identified as mesenchymal stem cells (MSCs) by their morphology and adherence on tissue culture flask. Cultured. Cultured ADSCs in differentiation-inducing medium until adipocytes, osteocytes and chondrocytes, and then added oil red O dye, alizarin red dye and Alcian blue dye (Sigma–Aldrich, USA) to stain the fixed differentiated cells. Cell surface marker antigens were detected with FACS Calibur fluorescence activated cell sorter (Becton Dickinson, USA), using anti-human CD31and CD105PE-conjugated antibodies (Becton Dickinson, USA) and anti-human CD90 PC5-conjugated antibodies (Becton Dickinson, USA).

Labeling of ADSCs

Carbocyanine lipophilic NIR fluorescent membrane dye, 1,1'-Dioctadecyl-3,3,3',3'-tetramethylindotricarbocyanine iodide (DiR, Aladdin, China) was used for labeling the cells. This fluorophore is excited at 748 nm and has an emission peak at 780 nm. A 5 μM final concentration of DiR was co-incubated with ADSCs (1×10^6 cells/ml Serum-free medium) at 37℃ for 30 min in the dark. Then, cells were centrifuged at 1000 rpm for 3 min at 4 ℃ and washed twice with PBS, resulting in a blue pellet. Labeled ADSCs were resuspended with hyaluronic acid (HA, Bloomage Biotech, China) at a density of 5×10^6 cell/ml for further experiment.

Apoptosis model in vitro and apoptosis inhibition

When the cells proliferated to 80–90% confluence, apoptosis was induced through treating ADSCs with 0.5 μM staurosporine (STS) (Beyotime, China) for 12 h. 50μM Z-VAD(OH)-FMK (MedChemExpress, USA), as inhibitor for caspase-3, was used to treat the cells at 1 h before they were treated with STS or used for in vivo experiments. Then the apoptosis ratio of STS-induced and apoptosis-inhibited ADSCs was detected by staining with TUNEL assay kit (Beyotime, China) and flow cytometry using PE Annexin V Apoptosis Detection Kit I (YEASEN, China) according to the manufacturer's manual. The inhibitory efficiency was analyzed by Eclipse Ti2-E fluorescent inverted microscope (Nikon, Japan), LSRfortessa flow cytometer (Becton Dickinson, USA) and FlowJo 10.0 software (Flow Jo LLC, USA).

Murine model of chronic radiation dermatitis and treatment with ADSCs

A preliminary experiment was conducted prior to the formal experiments to choose the proper radiation dosage for constructing CRD animal model. The mice (radiation group) were anaesthetized by inhalation of isoflurane. Then, with whole-body protection (lead plate), only full-thickness dorsal skin was exposed to radiation using an MBR-1505R2 irradiator (Hitachi Medical Corporation, Tokyo, Japan) through a single electron beam delivered by a Clinac iX linear accelerator (Varian Trilogy, USA). The total irradiation dose was 20 Gy β ray (dose rate of 2.86 Gy/min for 7 min) for one time. Five mice (control group) did not receive radiation. Dorsal areas were photographed at Weeks 1–9, to record cutaneous changes. The mice were sacrificed 9 weeks after radiation and the dorsal skin tissues were harvested.

In the formal experiment, to establish CRD model, mice were irradiated as described above. Fifty mice were randomly divided into irradiation plus HA (hyaluronic acid, Bloomade Biotech, China) (control group), and irradiation plus ADSCs (ADSCs group) ($n=25$ per group). At week 9 after receiving 20 Gy of irradiation, mice of ADSCs group received a multi-point intradermal injection within a $1.5\times1.5cm^2$ area delineated on the obviously injured dorsal skin using 1×10^5 DIR-labeled ADSCs (suspended in 0.2 ml HA). And the mice in control group were injected with equal dose of HA. The mice were sacrificed 0 day, 2 days, 5days, 4weeks and 8 weeks after the treatment and the dorsal skin tissues were harvested.

Thirty mice were randomly divided into irradiation plus ADSCs (ADSCs group) and irradiation plus 50μM ZVAD-pretreated ADSCs group (Z-VAD group) ($n=15$ per group). At week 9 after receiving 20 Gy of irradiation, mice of ADSCs group received a multi-point intradermal injection of 1×10^5 ADSCs (suspended in 0.2 ml HA). ADSCs used for mice in the ZVAD group were pretreated with 50μM Z-VAD 1 h before use. The mice were sacrificed 0 day, 4weeks and 8 weeks after the treatment and the dorsal skin tissues were harvested.

Assessment of CRD symptom severity

To evaluate the development of radiation-induced skin injury, the degree of skin tissue toxicity after irradiation was scored independently by two individuals who were blinded to the groups according to RTOG–EORTC and CTCAE criteria [12]. CRD symptom severity scores and pictures were recorded every two weeks until 8 weeks after the operation. Briefly, eight symptoms were evaluated: skin atrophy, erythema, exfoliation, oozing, crust, pigmentation change, skin induration, and telangiectasia, with a rating ranged from 0 (none) to 3 (severe) for each. The severity of CRD symptoms was determined as the sum scores.

Histologic analysis of skin sections

Skin samples were fixed with 4% paraformaldehyde for 24 h before they were embedded in paraffin. Paraffin sections (5 μm) were stained with hematoxylin-eosin (HE), Masson's Trichrome, and picrosirius red (Solarbio,

China) for morphology, fibrosis, and collagen typing assessment. The images of HE and Masson staining were scanned by SQS120P slide scanning imaging system (Shengqiang Technology, China). The images of picrosirius red staining were scanned by Eclipse microscope (Nikon, Japan) equipped with a polarizing filter.

TUNEL staining

TUNEL staining (Beyotime, China) was performed on 24-well culture plates (for cultured cells) or frozen sections (for tissues got at 2days and 5days after treatment) according to the manufacture's instruction. DAPI (Beyotime, China) was used for nuclear staining. The image collection was processed by Eclipse Ti2-E fluorescent inverted microscope (Nikon, Japan).

In vivo imaging

The animals were anaesthetized by inhalation of isoflurane and maintained in a prone position before the acquisition was started. In vivo fluorescence imaging was performed with Ami HTX small animal imaging system (Spectral instruments imaging, USA)0,1, 2, and 3 days after treatment. The fluorescence signals in the skin were quantified using Auro software (Spectral instruments imaging, USA).

Data processing of RNA-Seq

To reveal the molecular identities of CRD skin with transplanted ADSCs, we performed RNA sequencing on the CRD skin 8 weeks post HA treatment and CRD skin 8 weeks post ADSCs treatment. Total RNA was isolated using the Trizol Reagent (Invitrogen Life Technologies), after which the concentration, quality and integrity were determined using a NanoDrop spectrophotometer (Thermo Scientific). Sequencing was performed on NovaSeq 6000 platform (Illumina) Shanghai Personal Biotechnology Cp. Ltd. Each group contains three replicate samples.

Differentially expressed gene (DEG) analysis was performed by DESeq (v1.38.3) with screened conditions as follows: expression difference multiple |log2FoldChange| > 1, significant P-value < 0.05. At the same time, R language Pheatmap (v1.0.12) software package was used to perform bi-directional clustering analysis of all different genes of samples. Using topGO (v2.50.0) to perform gene ontology (GO) enrichment analysis on the differential genes (all DEGs / up DEGs / down DEGs), and find the GO term with significantly enriched differential genes to determine the main biological functions performed by differential genes.

Multiphoton image acquisition, and collagen morphologic feature extraction

Image acquisition for multiphoton imaging was performed with a 20× magnification on unstained serial section using FV1200MPE multiphoton imaging system (Olympus, Japan). We achieve second harmonic generation (SHG), which was separated by the dichroic mirror in the detection path. The channel corresponds to a wavelength range from 387 to 409 nm to present the microstructures of collagen fibers from the SHG signals.

Dermal collagen features were extracted drawing on the procedure of Chen et al. (2021) [23], which develop a collagen morphologic features extraction method of gastric cancer SHG image. Briefly, the extraction of collagen features was performed using MATLAB 2021a (MathWorks, USA). A total of 8 morphologic features, including mean and variance of collagen area, mean and variance of collagen length, mean and variance of collagen width, and mean and variance of collagen straightness, were extracted.

Statistical analysis

Data analysis was performed using OriginPro2021 (OriginLab, USA). Data are presented as mean ± Standard Error of Mean (SEM). Independent-sample t test, one-way ANOVA with Bonferroni's post hoc analysis, or two-way ANOVA with Bonferroni's post hoc analysis was used where appropriate. P-values less than 0.05 were considered statistically significant.

Results

Skin injury after radiation exposures in mice model: gross and microscopic assessments compared with CRD patients

To determine the appropriate irradiation dose for the CRD animal model and assess the similarity of cutaneous lesions in mice models with those in CRD clinical patients, we conducted gross inspections of exposed basal skin in mice for 9 weeks post-20 Gy irradiation. We then compared histologic sections (H&E, Masson stains, and Picrosirius red stains) between CRD patient skin ($n=5$) and mouse model skin samples ($n=5$).

At 9 weeks post-irradiation, CRD symptoms (skin atrophy, erythema, exfoliation, crust, pigmentation change, skin induration, and telangiectasia) were observed on irradiated areas of mice (Fig. 1A). H&E stains of skin samples at week 9 (Fig. 1B, below left) revealed epidermis hyperplasia, sebaceous gland hyperplasia, some areas of degeneration of collagen fibers, fibroblast proliferation and inflammatory cell infiltration in the dermis. Statistical analysis (Fig. 1D) showed that epidermal thickness of CRD group (80.42 ± 12.66 μm) was remarkably higher than that of the control group (31.69 ± 11.74 μm) ($p<0.001$). Masson stains at week 9 (Fig. 1B, below right) displayed subcutaneous lipoatrophy, altered collagen

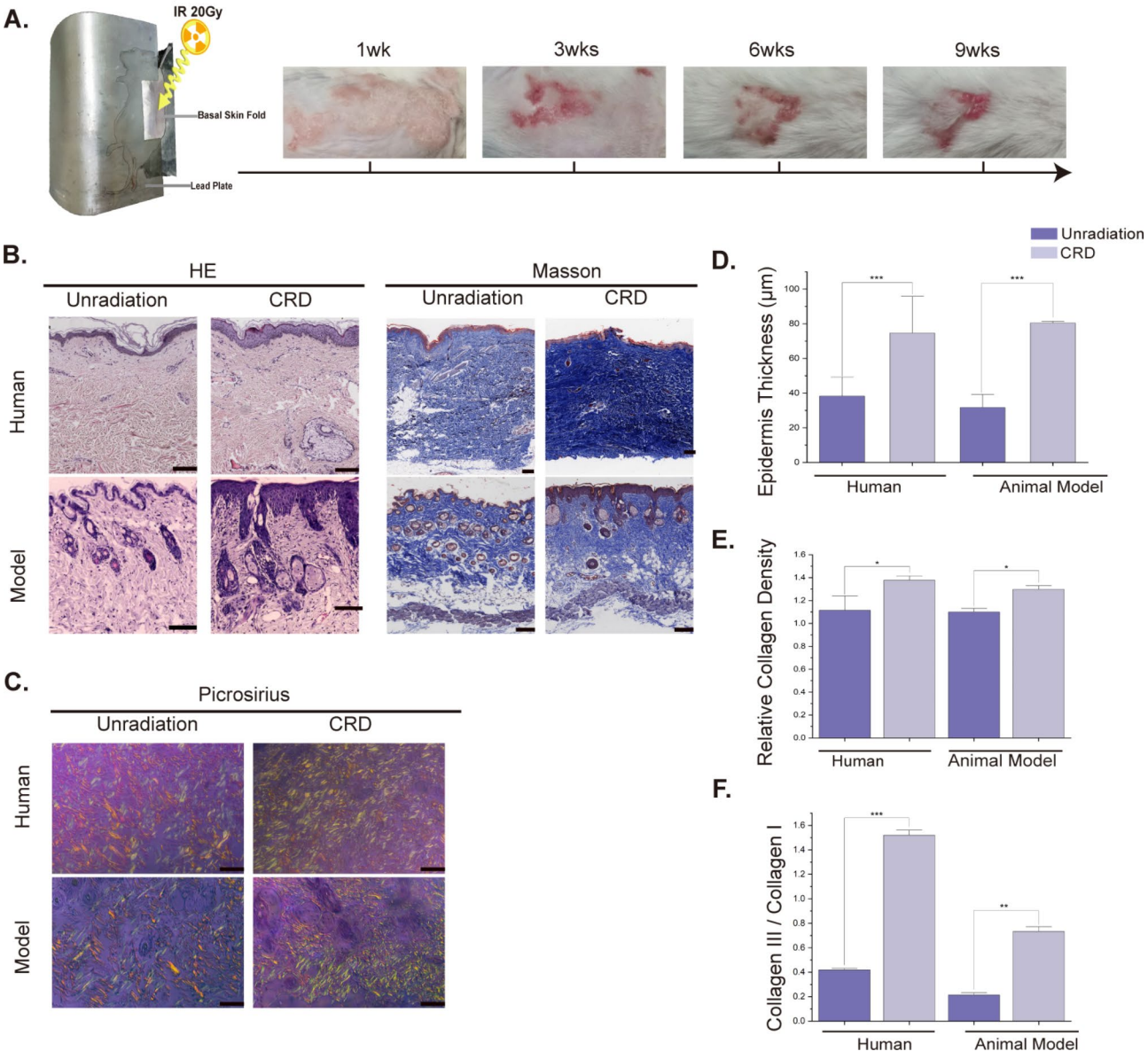

Fig. 1 Skin injury after radiation exposures in mice model: gross and microscopic assessments compared with CRD patients. **(A)** Representative photographs of mice dorsal skins, 1week, 3weeks, 6weeks, and 9weeks after receiving 20 Gy irradiation. **(B)** (Left) Photomicrographs of H&E-stained human and mice skin sections. Scale bar = 300 μm and 100 μm respectively. (Right) Photomicrographs of Masson-stained human and mice skin sections. Scale bar = 1 mm. **(C)** Photomicrographs of Picrosirius red-stained human and mice skin sections. Scare bar = 300 μm and 100 μm respectively. The green color indicates collagen III, while the yellow color indicates collagen I. **(D)** The analysis of epidermis thickness based on H&E staining. *** $p < 0.001$. **(E)** The analysis of relative collagen density based on Masson staining. *$P < 0.05$. **(F)** The analysis of ratio of Collagen III/Collagen I in dermis based on Picrosirius red-staining. **$p < 0.01$; *** $p < 0.001$

fiber structure with homogenization characteristic and increased relative collagen density of dermis (collagen density of dermis=collagen abundance/dermis thickness) (2.07±0.50 vs. 5.30±0.51, $p<0.001$) (Fig. 1E). Additionally, Picrosirius red stains at week 9 (Fig. 1C, below) indicated collagen I and III accumulation. The irradiation group exhibited more green color, indicating higher intensity of Collagen III. (0.21±0.02 vs. 0.73±0.03, $p<0.01$) (Fig. 1F).

These findings were consistent with histologic sections in CRD patients (Fig. 1B, upper; Fig. 1C, upper), in which the common pathological feathers, including acanthosis, fibrosis and irregular collagen deposition, could be summarized and representative. As reported by Malekzadeh [24] recently, they also found late radiation-induced skin fibrosis and irregular collagen deposition.

Transplanted ADSCs promote CRD skin regeneration

Aimed to explore whether ADSCs have a revitalizing effect in CRD, we compared the effect of HA (control group) and ADSCs (ADSCs group) (Fig. 2A). ADSCs were isolated from discarded fat of patients undergoing liposuction. Cultured ADSCs displayed a typical spindle shape (Fig. 2B), and their characterization was described in a previous study [22].

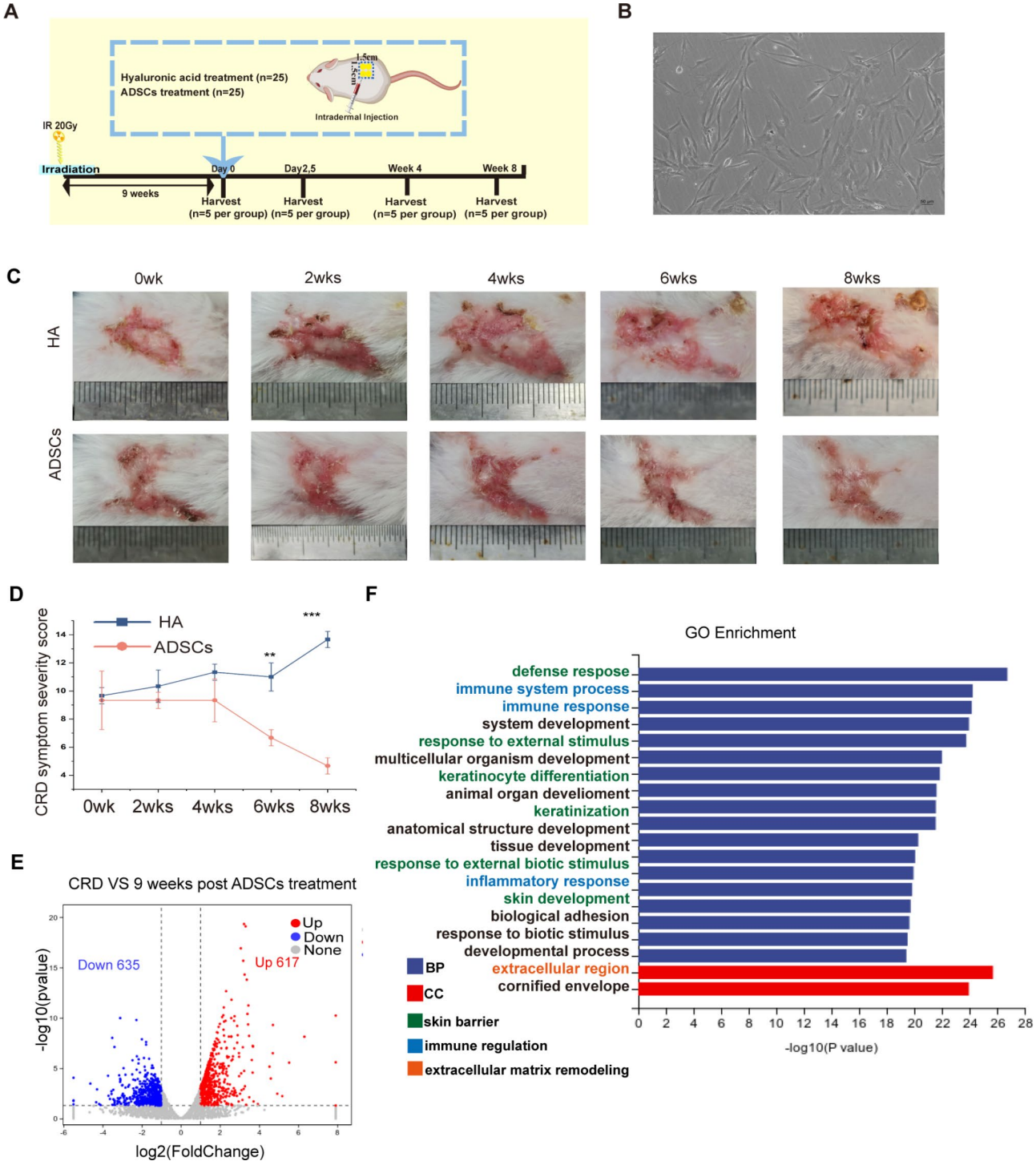

Fig. 2 Therapeutic effects of ADSCs on CRD skin regeneration. **(A)** Schematic of application of ADSCs. **(B)** Representative image of ADSCs. Scale bar = 50 μm. **(C)** Representative photographs of mice dorsal skins 0–8 weeks post HA and ADSCs treatment. **(D)** Statistical comparison of CRD symptom severity scores. $^{**}p < 0.01$; $^{***}p < 0.001$. **(E)** Volcano plots showing the gene expression profiles between the control group and the ADSCs group. **(F)** GO enrichment analysis plot showing significant regulated GO biological processes and cellular component items

In comparison with the control group, fewer chronic irradiation-induced skin injury symptoms were observed on the dorsal skin of ADSCs-treated mice during the 8 weeks post-treatment (Fig. 2C). In the control group, CRD symptom severity scores developed over time, whereas in the ADSCs group, symptom severity scores decreased over time (Fig. 2D).

To reveal the molecular identities of CRD skin with transplanted ADSCs, we performed RNA sequencing on the CRD skin 8 weeks post HA treatment (control group) and CRD skin 8 weeks post ADSCs treatment (ADSCs group). DGE analysis showed that 617 genes were highly expressed in the ADSC group, and 635 genes were highly expressed in the control group, which shows significant DEGs between control group and ADSCs group (|log2FoldChange| > 1; adjusted $P<0.05$) (Fig. 2E). GO enrichment results showed regulation of biological processes and cellular components important for skin regeneration such as extracellular matrix (ECM) remodeling, skin barrier establishment and immune regulation (Fig. 2F).

Further, to validate the therapeutic functions of ADSCs, histologic sections of skin tissues (harvested 0 day, 4 weeks and 8 weeks post-treatment) were evaluated. H&E-stained sections (Fig. 3A, left) showed that, ADSCs treatment attenuated epidermal thickening, irregular fibroblast proliferation, and inflammatory cell infiltration over time compared with the control group. Statistical analysis revealed a significant decrease in epidermal thickness in the ADSC group(57.18±2.78) vs. the control group (221.44±6.49) 8 weeks after treatment ($p<0.001$) (Fig. 3C). Additionally, the regenerated

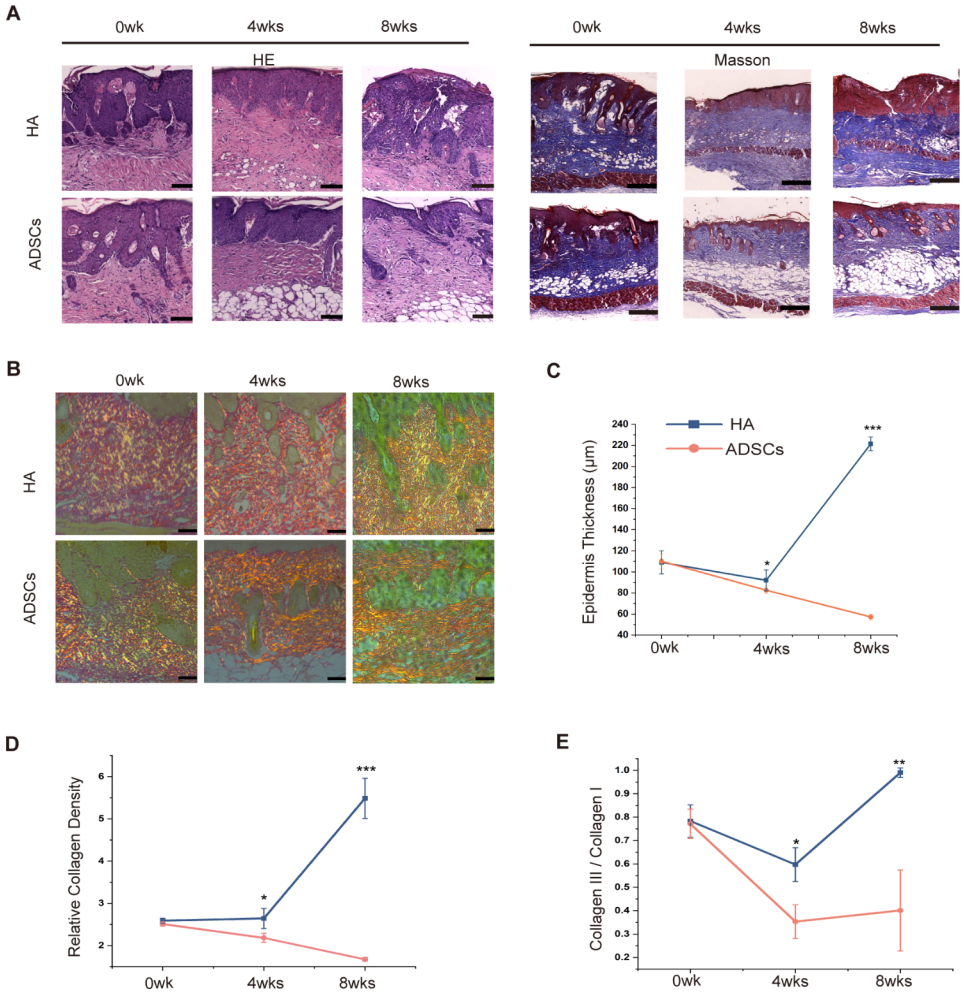

Fig. 3 Histologic sections analysis of effects of ADSCs on CRD skin regeneration. **(A)** (Left) photomicrographs of H&E-stained sections, 0week, 4 weeks and 8 weeks post treatment. Scare bar = 100 μm. (Right) photomicrographs of Masson-stained sections, 0week, 4 weeks and 8 weeks post treatment. Scare bar = 250 μm. **(B)** photomicrographs of Picrosirius red-stained sections, 0week, 4 weeks and 8 weeks post treatment. The green color indicates collagen III, while the yellow color indicates collagen I. Scare bar = 200 μm. **(C-E)** Statistical comparison of epidermis thickness **(C)**, relative collagen density **(D)** and the ratio of Collagen III/Collagen I **(E)** between HA treatment and ADSCs treatment at different time points post injection. *$p<0.05$; **$p<0.01$; *** $p<0.001$

subcutaneous fat appeared more substantial in the ADSCs group. In Masson-stained sections of tissues in the ADSCs group (Fig. 3A, right), remodeling of collagen fibers was observed, and fibroblasts proliferation and fiber production were suppressed over time. Statistical analysis showed that there was a significant decrease of relative collagen density (collagen density of dermis = collagen abundance/dermis thickness) in the ADSCs group(1.73 ± 0.05)vs. control group (5.38 ± 0.90) 8 weeks after treatment ($p < 0.001$) (Fig. 3D). Picrosirius red stains (Fig. 3B) revealed a decreased ratio of Collagen III / Collagen I in the dermis of the ADSCs group (0.40 ± 0.17) compared to the control group (0.99 ± 0.02) 8 weeks after treatment ($p < 0.01$) (Fig. 3E). In summary, histologic sections analysis showed the matched changes with the GO items suggested by RNA sequencing above.

Transplanted ADSCs underwent extensive apoptosis within few days

To explored the fate of ADSCs after transplantation, the In Vivo Imaging System was utilized to track DiR-labeled ADSCs post-injection (Fig. 4A), and In vivo images were quantified to determine the mean fluorescence radiant efficiency. Surprisingly, the fluorescence radiant

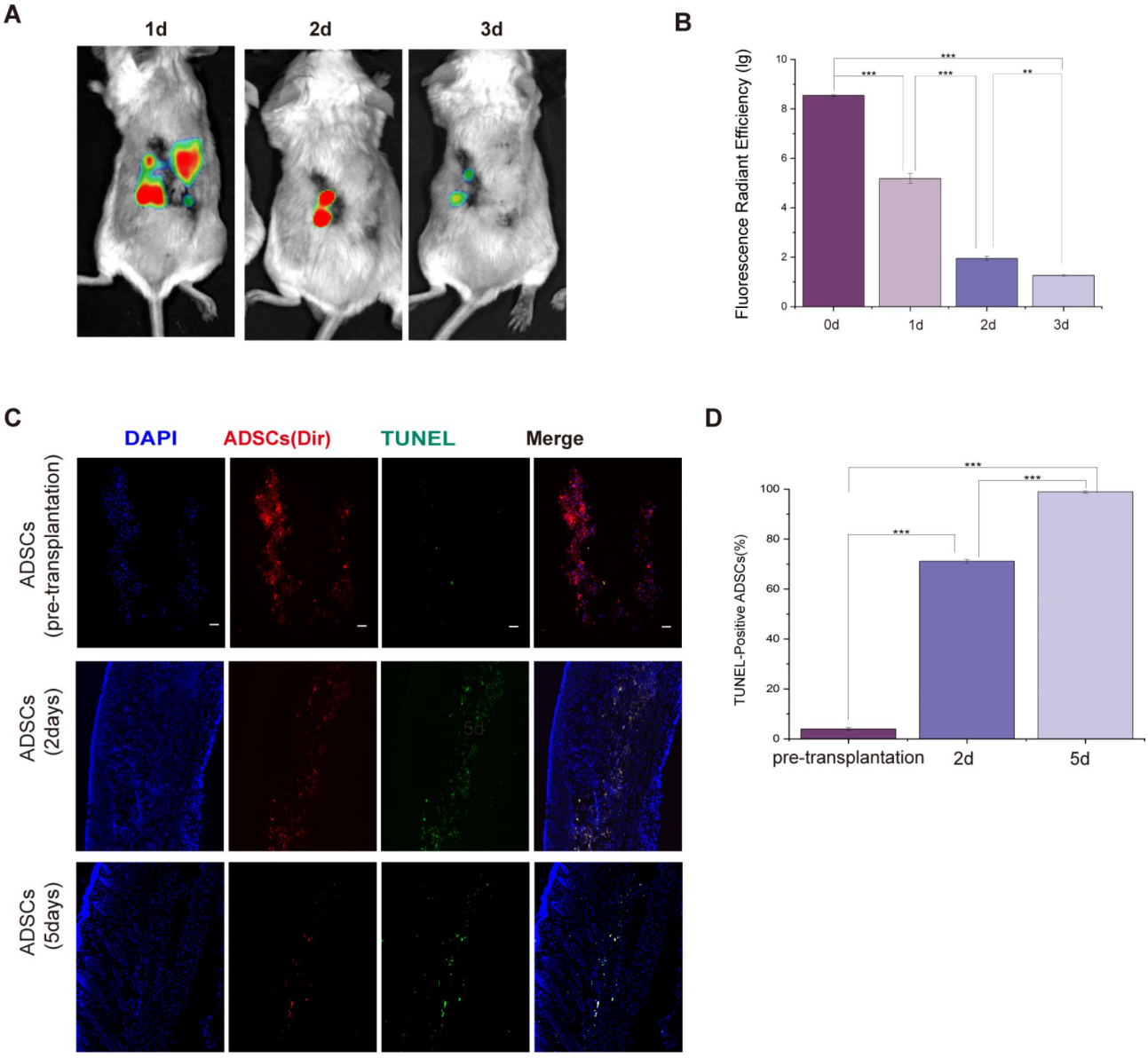

Fig. 4 Quantitative evaluation of ADSCs apoptosis rate after transplantation. **(A)** Representative time-dependent fluorescence images on postoperative day1, day2 and day3 for in vivo tracking of transplanted Dir-labeled ADSCs. **(B)** The quantitative analysis of fluorescence radiant efficiency at different time points post injection of ADSCs. $^{**}p < 0.01$; $^{***}p < 0.001$. **(C)** Dir-labeled ADSCs (red), and TUNEL-positive cells (green) at different time points post injection. Scare bar = 100 μm. **(D)** The analysis of the percentage of apoptotic ADSCs at different time points post injection, in TUNEL staining. $^{***}p < 0.001$

efficiency of DIR-labeled ADSCs significantly decreased over time (p<0.001) (Fig. 4B). Given the large decrease of ADSCs, we evaluated whether they were undergoing apoptosis. TUNEL staining (Fig. 4C) revealed that ADSCs became apoptotic after injection, with TUNEL-positive ADSCs reaching 71.16%±1.27% at 2 days post-injection and 98.94%±0.82% at 5 days post-injection (Fig. 4D). These results indicate that transplanted ADSCs undergo extensive apoptosis within a few days and are swiftly cleared from the injured site.

Apoptotic ADSCs are indispensable for CRD skin regeneration

Exploring the role of apoptosis in the therapeutic effect of ADSCs, we compared the effect of ADSCs (ADSCs group) and apoptosis-inhibited ADSCs (Z-VAD group) (Fig. 5A).

Initially, ADSCs in the Z-VAD group were pretreated with Z-VAD, an apoptosis inhibitor, and the inhibition efficiency was verified by comparing cell morphology under a light microscope (Fig. 5B) and flow cytometry (Fig. 5C). Furthermore, ADSCs and ADSCs pretreated with Z-VAD were injected in the dorsal skin of CRD mice.

Next, treatment effects of ADSCs and Z-VAD pretreated ADSCs were compared. In comparison with the Z-VAD group, fewer chronic irradiation-induced skin injury symptoms were observed on the dorsal skin of ADSCs-treated mice during the 8 weeks post- treatment (Fig. 6A). In the Z-VAD group, CRD symptom severity scores remained stable over time, whereas in the ADSCs-treated group, symptom severity scores decreased over time (Fig. 6D).

Histologic sections of skin tissues (harvested 0 week, 4 weeks and 8 weeks post-treatment) were evaluated. H&E-stained sections (Fig. 6B, left) showed that, ADSCs treatment attenuated epidermal thickening, irregular fibroblast proliferation, and inflammatory cell infiltration over time compared with the Z-VAD group. Statistical analysis revealed a significant decrease in epidermal thickness in the ADSCs group(58.23±2.33)vs. the Z-VAD group (146.82±17.74) 8 weeks after treatment (p<0.01) (Fig. 6E). In Masson-stained sections of tissues in the ADSC group (Fig. 6B, right), statistical analysis showed that there was a significant decrease of relative collagen density in the ADSCs group(1.67±0.17)vs. the Z-VAD group (2.32±0.27) 8 weeks after treatment (p<0.01) (Fig. 6F). Picrosirius red stains (Fig. 6C) revealed a

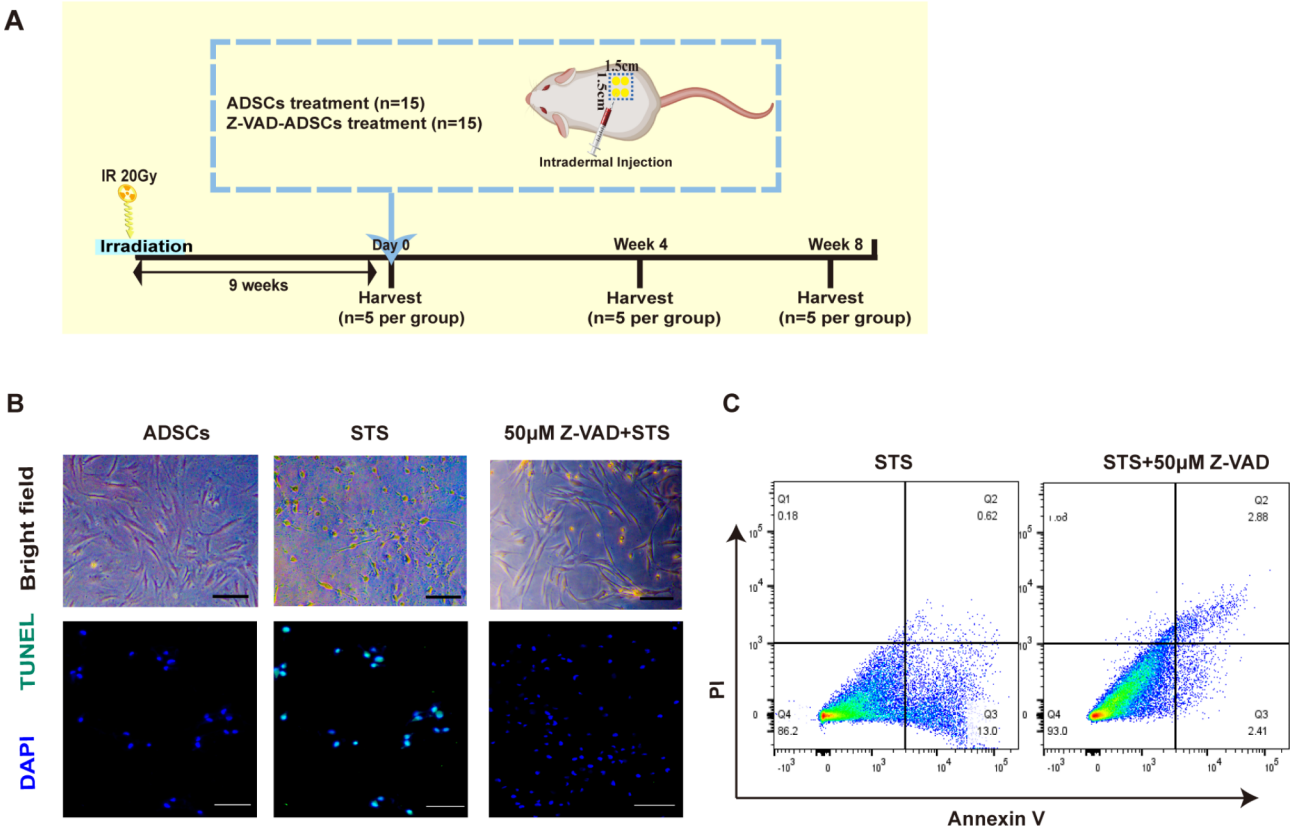

Fig. 5 Quantitative evaluation of the anti-apoptosis efficiency of Z-VAD in vitro. **(A)** Schematic of application of ADSCs and Z-VAD pretreated ADSCs. **(B, C)** the STS treatment induced the apoptosis of ADSCs, which was attenuated by pretreatment of Z-VAD, an inhibitor of caspase-3. The anti-apoptosis efficiency of Z-VAD in vitro was analyzed by morphological changes **(B**, Above**)**, TUNEL staining **(B**, Below**)** and flow cytometry **(C)**

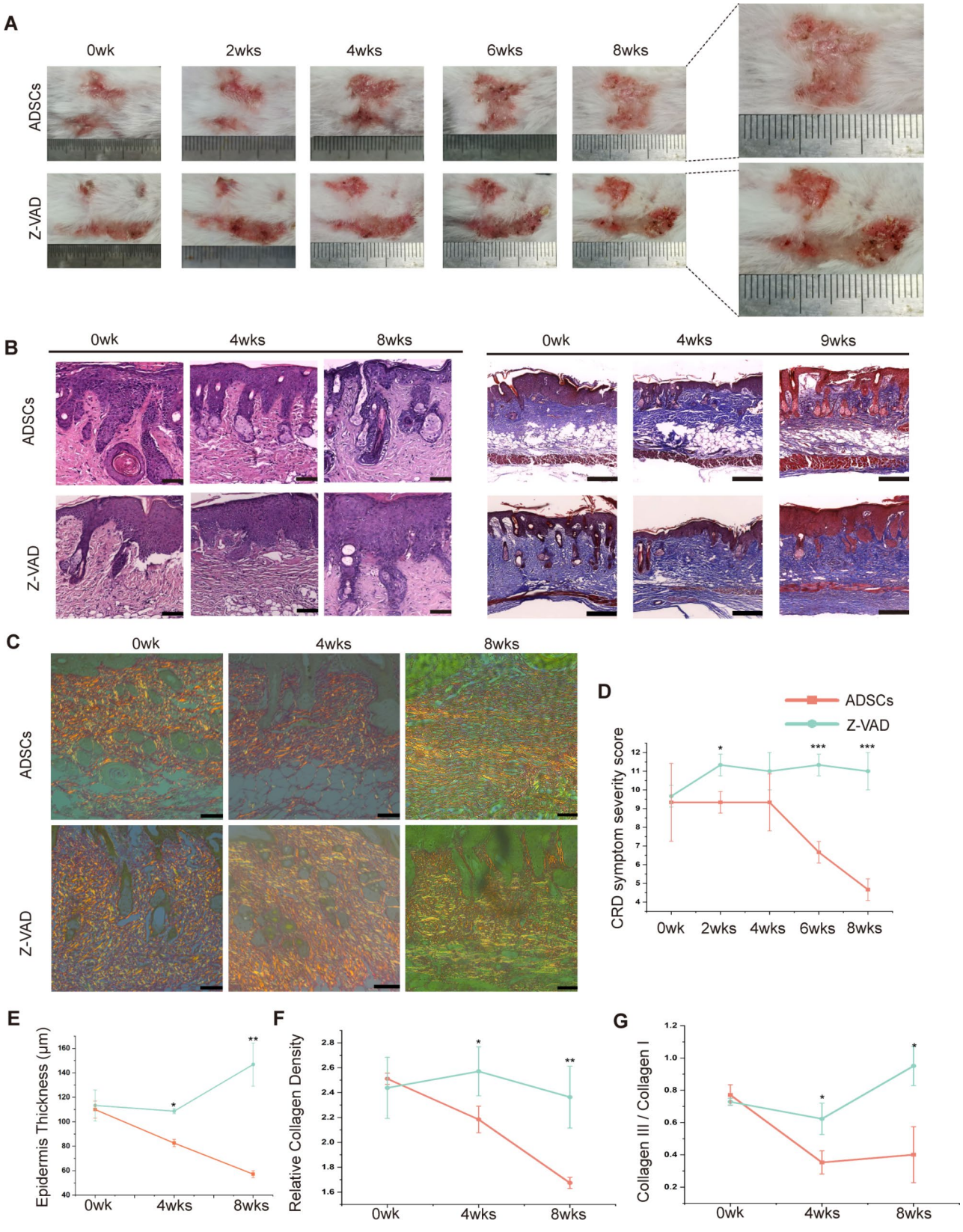

Fig. 6 (See legend on next page.)

(See figure on previous page.)

Fig. 6 Comparison of therapeutic effects of ADSCs and Z-VAD pretreated ADSCs on CRD skin regeneration. **(A)** Representative photographs of mice dorsal skins 0–8 weeks post ADSCs and Z-VAD-pretreated ADSCs treatment. **(B)** (Left) photomicrographs of H&E-stained sections, 0week, 4 weeks and 8 weeks post treatment. Scare bar = 100 μm. (Right) photomicrographs of Masson-stained sections, 0week, 4 weeks and 8 weeks post treatment. Scare bar = 250 μm. **(C)** photomicrographs of Picrosirius red-stained sections, 0week, 4 weeks and 8 weeks post treatment. The green color indicates collagen III, while the yellow color indicates collagen I. Scare bar = 200 μm. **(D-G)** Statistical comparison of CRD symptom severity scores **(D)**, epidermis thickness **(E)**, relative collagen density **(F)** and the ratio of Collagen III/Collagen I **(G)** between ADSCs treatment and Z-VAD pretreated ADSCs treatment at different time points post injection. *$p < 0.05$; **$p < 0.01$; *** $p < 0.001$

decreased ratio of Collagen III / Collagen I in the dermis of the ADSCs-treated group (0.42±0.15) compared to the Z-VAD group (0.92±0.11) 8 weeks after treatment (p<0.05) (Fig. 6G).

In summary, these therapeutic effects of ADSCs were attenuated by Z-VAD (apoptosis inhibitor). These data demonstrated the therapeutic effects of transplanted ADSCs on CRD, partially governed by apoptosis.

The therapeutic potential of MSCs in tissue repair was discovered decades. And it is recognized that various positive effects of MSCs are mainly attributed to their paracrine factors in vivo, like growth factors, anti-inflammatory cytokines, pro-angiogenic factors, anti-fibrotic factors inhibitor proteins of apoptosis, and nerve growth factors [25]. In this study, apoptosis emerges as a possible key method through which ADSCs release therapeutic paracrine factors in vivo, which contributed to ECM remodeling, skin barrier establishment and immune regulation in late radiation-induced skin regeneration.

Apoptotic ADSCs: remodeling and rearranging dermal collagens matrix for late radiation-induced skin regeneration

Collagen is one of the main components of ECM in the dermis. Tissue remodeling and collagen degradation is necessary for skin repair and regeneration [26]. SHG images of histologic sections (Fig. 7A) showed that CRD induced collagen atrophy and rupture, resulting in a disordered collagen network.

The collagen morphological features extraction framework is presented in Fig. 7B. A total of eight collagen morphological features, including mean and variance of collagen area, mean and variance of collagen length, mean and variance of collagen width, and mean and variance of collagen straightness, were extracted from SHG image using MATLAB. Statistical analysis (Fig. 7C) demonstrated significantly decreased mean of collagen area, mean of collagen length, variance of collagen length, variance of collagen width, and variance of collagen straightness in CRD compared to unirradiated tissue. Mean of collagen straightness was significantly increased in CRD compared to unirradiated tissue. These alterations support the notion that CRD induces collagen atrophy and rupture. ADSCs treatment could enlarge, lengthen, crimp and even collagen, while apoptosis inhibition attenuated these therapeutic effects. These results indicate that transplanted ADSCs can help remodel the dysfunctional ECM of the skin dermis by restoring a normal collagen network when undergoing apoptosis.

Discussion

In this study, we demonstrated the potential of ADSCs in treating radiation-induced skin injuries. As the transcriptome profiling results in our study shows, ADSCs may contribute to extracellular matrix remodeling, skin barrier establishment and immune regulation in late radiation-induced skin regeneration. Histological sections analysis validated the therapeutic effects of ADSCs, including alleviating symptoms, acanthosis of the epidermis, dermal fibrosis, and alterations in the Collagen III/Collagen I ratio and modifying collagen morphological signatures. Of particular interest, when we monitored the fate of transplanted ADSCs after transplantation, we made a surprising observation that these cells underwent extensive apoptosis within a few days. Furthermore, our study indicated that the therapeutic effects of ADSCs were diminished by the presence of an apoptosis inhibitor (Fig. 8). Our study aligns with recent findings that MSCs will undergo extensive apoptosis within few days, but continue to exhibit beneficial effects through paracrine secretion a variety of substances [27–31]. Several animal studies seem to indicate that autocrine or paracrine effects of MSCs rather than their direct engraftment and tissue differentiation may play the key role in wound healing and tissue repair [32–34]. In summary, our study illustrated that apoptosis maybe one of the mainly methods for ADSCs releasing related therapeutic paracrine factors.

Apoptotic cells can release a variety of substances including metabolites and apoptotic extracellular vesicles (ApoEVs, a main subtype of extracellular vesicles). As reported, ApoEVs could activate autophagy in recipient cells to induce angiogenesis and dental pulp regeneration [35]. We supposed that apoptotic ADSCs may also exert therapeutic effects on CRD skin through ApoEVs, which deserved further exploring. In addition, biomaterials, like scaffold, hydrogel s might serve as a biomimetic structure inspired by the natural environment, assisting stem cells or their extracellular vesicles in establishing their natural relationships and playing a better regenerative effect, which can be targeted in future therapeutic strategies [36–39].

A significant finding in our research was the irregular collagen deposition and increased Collagen III/Collagen

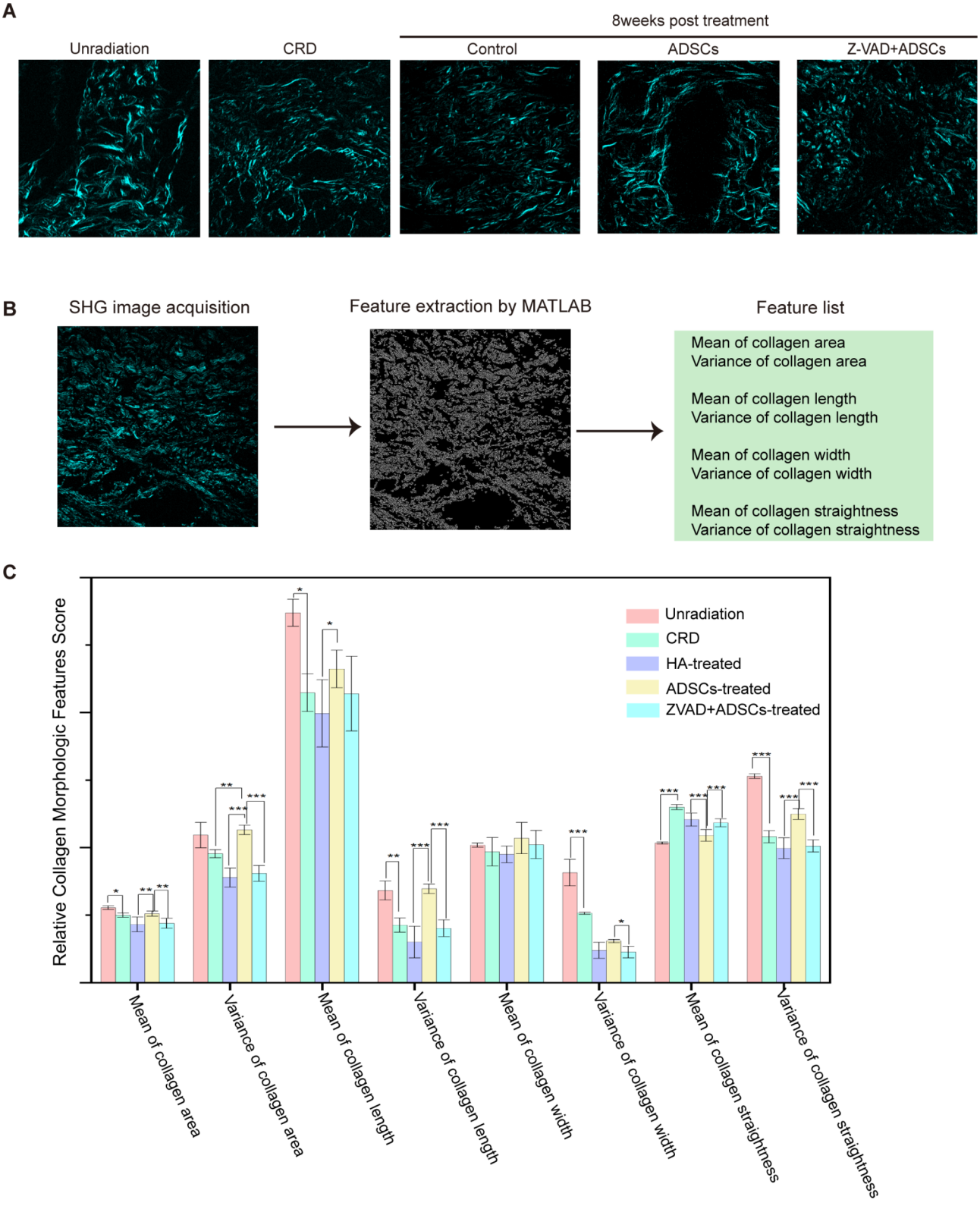

Fig. 7 Quantitative evaluation of collagen morphological features. **(A)** SHG image of dermis of normal skin, CRD skin and CRD skin post 8 weeks different treatment. **(B)** Framework of the collagen morphological features extraction. (Left) Acquisition of second harmonic generation (SHG) combined images. Three representative regions of every sample, with a field of view of 1024 × 1024, were selected to obtain the corresponding multiphoton imaging. (Medium) The SHG image was used for collagen feature extraction. (Right) A total of eight collagen features were selected and used for statistical comparison **(C)** Statistical comparison of eight collagen features. *$p < 0.05$'**$p < 0.01$; *** $p < 0.001$

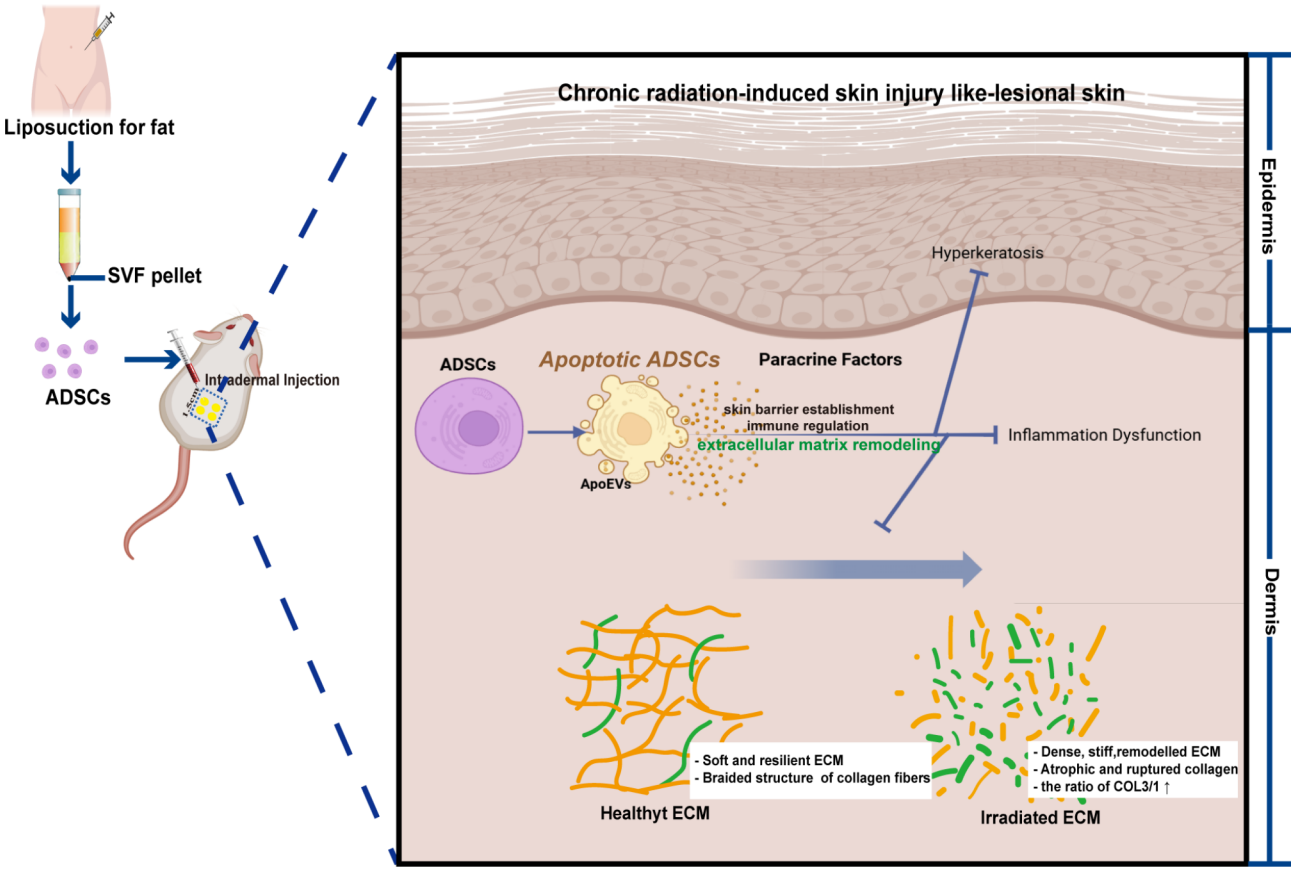

Fig. 8 Illustration of the therapeutic mechanisms of apoptotic ADSCs on CRD

I ratio in CRD skin, which transplanted ADSCs demonstrated the ability to decrease. Collagen is one of the main components of ECM in the dermis. Reorganization of newly synthesized collagen is the final and important stage during skin healing and regeneration [40]. Skin fibrotic disease is characterized by excessive and uncontrolled synthesis of ECM proteins, especially collagens [41]. Among the 28 types of collagens with characteristic tissue distribution and function, Collagen I and Collagen III, also known as fibrillar collagens, are distributed mainly in the ECM of the skin tissue [42]. Regenerative medicine in the treatment of specific skin disorders has undergone extensive research in clinical trials for treating specific skin disorders [43]. The effect of ADSCs on irregular collagen deposition when alleviating skin fibrotic diseases like hypertrophic scarring and keloids has been widely reported. Wang et al [44]. showed that co-culture of keloid tissue with ADSC-conditioned medium in vitro could significantly reduce the expression of tissue inhibitor of metalloproteinases-1 (TIMP1) and the deposition of Collagen I in keloid tissue. Similarly, Zhang et al [45]. injected ADSCs into rabbit ear lesions resulted in reducing the formation of rabbit ear hypertrophic scars by decreasing the α-SMA and Collagen I gene expression and ameliorating collagen deposition. Additionally, it has been shown that the ratio of Collagen III/ Collagen I increases in certain skin fibrotic diseases such as keloids, grade-3 lymphoedema, and diabetic wounds [46–48].

The often-overlooked changes in collagen fiber network morphology and texture can influence ECM remodeling. As researches report, modifications of collagen, like stiff and dense, mineralization, cross-linking via advanced glycation end-products, and the removal or addition of glycosaminoglycans, have a direct impact on its degradation [49–51]. Thus, alterations in collagen morphology induced by radiation rays might contribute to the challenges in treating CRD. In this research, we observed that irradiation induced collagen atrophy and rupture, while ADSCs could enlarge, lengthen, crimp and even the damaged collagen.

Normal structured collagen network may contribute to the soft and plastic texture of normal skin through providing appropriate rigidity, while damaged collagen network caused the stiffness of CRD skin. Serving as structural support, collagen's rigidity influences various cell behaviors, impacting pathophysiological phenomena ranging from development and differentiation to repair and regeneration of diseased and damaged tissues

through so-called 'mechanosensing process' [52, 53]. As recent researches report, appropriate collagen rigidity can induce adipogenesis of MSCs into adipocyte-like cells, [54] and contributes towards an exceptional ordering of its hydration water [55]. Therefore, normal structured collagen network may contribute to the soft and plastic texture of normal skin through providing appropriate rigidity, while damaged collagen network caused the stiffness of CRD skin.

Conclusion

We demonstrate that ADSCs undergo extensive apoptosis after local skin transplantation, and apoptosis is a requirement for ADSCs efficacy in promoting radiation-impaired skin regeneration mainly via remodeling and rearranging dermal collagens matrix.

Abbreviations

ADSCs	Adipose-Derived Stem Cells
ApoEVs	Apoptotic Extracellular Vesicles
CRD	Chronic Radiation Dermatitis
ECM	Extracellular Matrix
EVs	Extracellular Vesicles
MSCs	Mesenchymal Stem Cells

Supplementary Information

The online version contains supplementary material available at https://doi.org/10.1186/s13287-024-03904-z.

Supplementary Material 1

Acknowledgements

The authors declare that they have not used Artificial Intelligence in this study.

Author contributions

YFZ, XL helped in methodology, collection of data, data analysis, and manuscript writing. XHC helped in supervision and writing. XHC and YJL helped in concept and design, manuscript writing, and final approval of the manuscript.

Funding

The authors gratefully acknowledge the support for this study from the National Natural Science Foundation of China (Nos. 81971852 and 82202476).

Data availability

All relevant data are included in the manuscript and supplementary material.

Declarations

Ethics approval

The experiment titled 'Study on the therapeutic effects of ADSCs on chronic radiation-induced skin injury' involves animal experimentation and has been approved by the Ethics Committee of Nanfang Hospital, Southern Medical University. The Ethics Committee approved this experimental project on November 21, 2022, with the approval number IACUC-LAC-20221121-003. All experimental procedures will strictly adhere to the approved documents of the Ethics Committee, ensuring proper care of the animals and compliance with animal welfare regulations.

Consent for publication

All authors read and approved the manuscript.

Patient consent

This study was approved by the Medical Ethics Committee of Nanfang Hospital, Southern Medical University (NFEC-2023-355), and each patient signed an informed consent for providing discarded human breast skin tissue or human adipose tissue.

Competing interests

The authors declare that they have no competing interests.

Author details

[1]Department of Plastic Surgery, Nanfang Hospital, Southern Medical University, 1838 Guangzhou North Road, Guangzhou 510515, Guangdong, People's Republic of China

Received: 23 July 2024 / Accepted: 26 August 2024
Published online: 27 September 2024

References

1. Montazersaheb S, Jafari S, Aytemir MD, Ahmadian E, Ardalan M, Zor M, et al. The synergistic effects of betanin and radiotherapy in a prostate cancer cell line: an in vitro study. Mol Biol Rep. 2023;50(11):9307–14.
2. Haussmann J, Corradini S, Nestle-Kraemling C, Bölke E, Njanang FJD, Tamaskovics B, et al. Recent advances in radiotherapy of breast cancer. Radiat Oncol. 2020;15(1):71.
3. Hickok JT, Morrow GR, Roscoe JA, Mustian K, Okunieff P. Occurrence, severity, and longitudinal course of twelve common symptoms in 1129 consecutive patients during radiotherapy for cancer. J Pain Symptom Manag. 2005;30(5):433–42.
4. Ryan JL. Ionizing radiation: the good, the bad, and the ugly. J Invest Dermatol. 2012;132(3 Pt 2):985–93.
5. Bray FN, Simmons BJ, Wolfson AH, Nouri K. Acute and chronic cutaneous reactions to Ionizing Radiation Therapy. Dermatology Therapy. 2016;6(2):185–206.
6. Wong RK, Bensadoun RJ, Boers-Doets CB, Bryce J, Chan A, Epstein JB, et al. Clinical practice guidelines for the prevention and treatment of acute and late radiation reactions from the MASCC skin toxicity Study Group. Supportive care cancer: Official J Multinational Association Supportive Care Cancer. 2013;21(10):2933–48.
7. Hymes SR, Strom EA, Fife C. Radiation dermatitis: clinical presentation, pathophysiology, and treatment 2006. J Am Acad Dermatol. 2006;54(1):28–46.
8. Bernier J, Bonner J, Vermorken JB, Bensadoun RJ, Dummer R, Giralt J, et al. Consensus guidelines for the management of radiation dermatitis and coexisting acne-like rash in patients receiving radiotherapy plus EGFR inhibitors for the treatment of squamous cell carcinoma of the head and neck. Annals Oncology: Official J Eur Soc Med Oncol. 2008;19(1):142–9.
9. Denham JW, Hauer-Jensen M. The radiotherapeutic injury–a complex 'wound'. Radiotherapy Oncology: J Eur Soc Therapeutic Radiol Oncol. 2002;63(2):129–45.
10. Cox JD, Stetz J, Pajak TF. Toxicity criteria of the Radiation Therapy Oncology Group (RTOG) and the European Organization for Research and Treatment of Cancer (EORTC). Int J Radiat Oncol Biol Phys. 1995;31(5):1341–6.
11. Sullivan SR, Fletcher DRD, Isom CD, Isik FF. True incidence of all complications following immediate and delayed breast reconstruction. Plast Reconstr Surg. 2008;122(1):19–28.
12. Spałek M. Chronic radiation-induced dermatitis: challenges and solutions. Clin Cosmet Invest Dermatology. 2016;9:473–82.
13. Zasadziński K, Spałek MJ, Rutkowski P. Modern dressings in Prevention and Therapy of Acute and Chronic Radiation Dermatitis-A Literature Review. Pharmaceutics. 2022;14(6).
14. Borrelli MR, Shen AH, Lee GK, Momeni A, Longaker MT, Wan DC. Radiation-Induced skin fibrosis: Pathogenesis, Current Treatment options, and emerging therapeutics. Ann Plast Surg. 2019;83(4S Suppl 1):S59–64.
15. Huayllani MT, Ruiz-Garcia H, Boczar D, Avila FR, Lu X, Rinker BD, et al. Adipose-derived stem cells therapy for Radiation-Induced skin Injury. Ann Plast Surg. 2021;87(6):639–49.
16. Luan A, Duscher D, Whittam AJ, Paik KJ, Zielins ER, Brett EA, et al. Cell-assisted Lipotransfer improves volume Retention in Irradiated Recipient sites and rescues Radiation-Induced skin changes. Stem cells (Dayton. Ohio). 2016;34(3):668–73.

17. Wu SH, Shirado T, Mashiko T, Feng J, Asahi R, Kanayama K, et al. Therapeutic effects of Human adipose-derived products on impaired Wound Healing in irradiated tissue. Plast Reconstr Surg. 2018;142(2):383–91.
18. Sultan SM, Stern CS, Allen RJ Jr., Thanik VD, Chang CC, Nguyen PD, et al. Human fat grafting alleviates radiation skin damage in a murine model. Plast Reconstr Surg. 2011;128(2):363–72.
19. Li S, Sun J, Yang J, Yang Y, Ding H, Yu B, et al. Gelatin methacryloyl (GelMA) loaded with concentrated hypoxic pretreated adipose-derived mesenchymal stem cells(ADSCs) conditioned medium promotes wound healing and vascular regeneration in aged skin. Biomater Res. 2023;27(1):11.
20. Liu YX, Sun JM, Ho CK, Gao Y, Wen DS, Liu YD, et al. Advancements in adipose-derived stem cell therapy for skin fibrosis. World J Stem Cells. 2023;15(5):342–53.
21. Mende W, Götzl R, Kubo Y, Pufe T, Ruhl T, Beier JP. The role of adipose stem cells in bone regeneration and bone tissue Engineering. Cells. 2021;10(5).
22. Liu L, Gao J, Yuan Y, Chang Q, Liao Y, Lu F. Hypoxia preconditioned human adipose derived mesenchymal stem cells enhance angiogenic potential via secretion of increased VEGF and bFGF. Cell Biol Int. 2013;37(6):551–60.
23. Chen D, Chen H, Chi L, Fu M, Wang G, Wu Z, et al. Association of Tumor-Associated Collagen Signature with prognosis and adjuvant chemotherapy benefits in patients with gastric Cancer. JAMA Netw open. 2021;4(11):e2136388.
24. Malekzadeh H, Surucu Y, Chinnapaka S, Yang KS, Arellano JA, Samadi Y, et al. Metformin and adipose-derived stem cell combination therapy alleviates radiation-induced skin fibrosis in mice. Stem Cell Res Ther. 2024;15(1):13.
25. Vizoso FJ, Eiro N, Cid S, Schneider J, Perez-Fernandez R. Mesenchymal stem cell secretome: toward cell-free therapeutic strategies in Regenerative Medicine. Int J Mol Sci. 2017;18(9).
26. Lu P, Takai K, Weaver VM, Werb Z. Extracellular matrix degradation and remodeling in development and disease. Cold Spring Harb Perspect Biol. 2011;3(12).
27. Liu S, Jiang L, Li H, Shi H, Luo H, Zhang Y, et al. Mesenchymal stem cells prevent hypertrophic scar formation via inflammatory regulation when undergoing apoptosis. J Invest Dermatol. 2014;134(10):2648–57.
28. Pang SHM, D'Rozario J, Mendonca S, Bhuvan T, Payne NL, Zheng D, et al. Mesenchymal stromal cell apoptosis is required for their therapeutic function. Nat Commun. 2021;12(1):6495.
29. Laing AG, Riffo-Vasquez Y, Sharif-Paghaleh E, Lombardi G, Sharpe PT. Immune modulation by apoptotic dental pulp stem cells in vivo. Immunotherapy. 2018;10(3):201–11.
30. Fu Y, Sui B, Xiang L, Yan X, Wu D, Shi S, et al. Emerging understanding of apoptosis in mediating mesenchymal stem cell therapy. Cell Death Dis. 2021;12(6):596.
31. Kholodenko IV, Kholodenko RV, Majouga AG, Yarygin KN. Apoptotic MSCs and MSC-Derived apoptotic bodies as New Therapeutic Tools. Curr Issues Mol Biol. 2022;44(11):5153–72.
32. Ranganath SH, Levy O, Inamdar MS, Karp JM. Harnessing the mesenchymal stem cell secretome for the treatment of cardiovascular disease. Cell Stem Cell. 2012;10(3):244–58.
33. Stastna M, Van Eyk JE. Investigating the secretome: lessons about the cells that comprise the heart. Circulation Cardiovasc Genet. 2012;5(1):o8–18.
34. Drago D, Cossetti C, Iraci N, Gaude E, Musco G, Bachi A, et al. The stem cell secretome and its role in brain repair. Biochimie. 2013;95(12):2271–85.
35. Li Z, Wu M, Liu S, Liu X, Huan Y, Ye Q, et al. Apoptotic vesicles activate autophagy in recipient cells to induce angiogenesis and dental pulp regeneration. Mol Ther. 2022;30(10):3193–208.
36. Dong Y, Cui M, Qu J, Wang X, Kwon SH, Barrera J, et al. Conformable hyaluronic acid hydrogel delivers adipose-derived stem cells and promotes regeneration of burn injury. Acta Biomater. 2020;108:56–66.
37. Shahi S, Dehghani F, Abdolahinia ED, Sharifi S, Ahmadian E, Gajdács M, et al. Effect of gelatinous spongy scaffold containing nano-hydroxyapatite on the induction of odontogenic activity of dental pulp stem cells. J King Saud Univ - Sci. 2022;34(8):102340.
38. Wu D, Tao S, Zhu L, Zhao C, Xu N. Chitosan Hydrogel Dressing Loaded with adipose mesenchymal stem cell-derived Exosomes promotes skin full-thickness Wound Repair. ACS Appl Bio Mater. 2024;7(2):1125–34.
39. Zhang X, Yang J, Ma S, Gao X, Wang G, Sun Y, et al. Functional diversity of apoptotic vesicle subpopulations from bone marrow mesenchymal stem cells in tissue regeneration. J Extracell Vesicles. 2024;13(4):e12434.
40. Xue M, Jackson CJ. Extracellular matrix reorganization during Wound Healing and its impact on abnormal scarring. Adv Wound care. 2015;4(3):119–36.
41. Zhao X, Psarianos P, Ghoraie LS, Yip K, Goldstein D, Gilbert R, et al. Metabolic regulation of dermal fibroblasts contributes to skin extracellular matrix homeostasis and fibrosis. Nat Metabolism. 2019;1(1):147–57.
42. Smith LT, Holbrook KA, Madri JA. Collagen types I, III, and V in human embryonic and fetal skin. Am J Anat. 1986;175(4):507–21.
43. Jafarzadeh A, Pour Mohammad A, Keramati H, Zeinali R, Khosravi M, Goodarzi A. Regenerative medicine in the treatment of specific dermatologic disorders: a systematic review of randomized controlled clinical trials. Stem Cell Res Ther. 2024;15(1):176.
44. Wang X, Ma Y, Gao Z, Yang J. Human adipose-derived stem cells inhibit bioactivity of keloid fibroblasts. Stem Cell Res Ther. 2018;9(1):40.
45. Zhang Q, Liu LN, Yong Q, Deng JC, Cao WG. Intralesional injection of adipose-derived stem cells reduces hypertrophic scarring in a rabbit ear model. Stem Cell Res Ther. 2015;6(1):145.
46. Macarak EJ, Wermuth PJ, Rosenbloom J, Uitto J. Keloid disorder: fibroblast differentiation and gene expression profile in fibrotic skin diseases. Exp Dermatol. 2021;30(1):132–45.
47. Karayi AK, Basavaraj V, Narahari SR, Aggithaya MG, Ryan TJ, Pilankatta R. Human skin fibrosis: up-regulation of collagen type III gene transcription in the fibrotic skin nodules of lower limb lymphoedema. Tropical medicine & international health: TM & IH. 2020;25(3):319 – 27.
48. Zhao X, Fu L, Zou H, He Y, Pan Y, Ye L, et al. Optogenetic engineered umbilical cord MSC-derived exosomes for remodeling of the immune microenvironment in diabetic wounds and the promotion of tissue repair. J Nanobiotechnol. 2023;21(1):176.
49. Goldin A, Beckman JA, Schmidt AM, Creager MA. Advanced glycation end products: sparking the development of diabetic vascular injury. Circulation. 2006;114(6):597–605.
50. Wood LK, Kayupov E, Gumucio JP, Mendias CL, Claflin DR, Brooks SV. Intrinsic stiffness of extracellular matrix increases with age in skeletal muscles of mice. J Appl Physiol (Bethesda Md: 1985). 2014;117(4):363–9.
51. Panwar P, Butler GS, Jamroz A, Azizi P, Overall CM, Brömme D. Aging-associated modifications of collagen affect its degradation by matrix metalloproteinases. Matrix Biology: J Int Soc Matrix Biology. 2018;65:30–44.
52. Discher DE, Janmey P, Wang YL. Tissue cells feel and respond to the stiffness of their substrate. Sci (New York NY). 2005;310(5751):1139–43.
53. Shaw TJ, Martin P. Wound repair at a glance. J Cell Sci. 2009;122(Pt 18):3209–13.
54. Moreno-Castellanos N, Cuartas-Gómez E, Vargas-Ceballos O. Collagen-mesenchymal stem cell spheroids in suspension promote high adipogenic capacity. Biomedical Mater (Bristol England). 2023;18(4).
55. Biswal S, Agmon N. Collagen Structured Hydration. Biomolecules. 2023;13(12).

Publisher's note